Helicon waves and efficient plasma production

A. Komori, T. Shoji,[a] K. Miyamoto, J. Kawai, and Y. Kawai
Interdisciplinary Graduate School of Engineering Sciences, Kyushu University, Kasuga, Fukuoka 816, Japan

(Received 13 August 1990; acccepted 31 December 1990)

Helicon waves generated by radio-frequency (rf) waves are experimentally demonstrated to have the characteristics of Landau damping, as predicted theoretically, and fully ionized plasmas are realized by this efficient coupling of rf powers to plasmas. Excited waves are identified as a helicon wave by measuring wavelengths in the plasma along the magnetic field and comparing with the dispersion relation. Good agreement is found between experimental and theoretical results.

I. INTRODUCTION

The plasma production by radio-frequency (rf) waves using either inductive or capacitive coupling methods has been well known to realize appreciable high density and temperature plasmas easily. Rather than simply relying on the large oscillatory electric fields of the antenna to accelerate electrons to ionizing energies, resonant excitation methods have been found to be more effective.[1] Recent experiments by Boswell *et al.*[2–4] have shown that fully ionized plasmas whose density is higher than 1×10^{12} cm^{-3} can be produced with a special antenna to excite a helicon wave in a chamber of 10 cm in diameter and 120 cm in length with an rf power of 180 W at 8.8 MHz and a confining magnetic field of 0.75 kG. It has been shown that wave properties are consistent with those expected of helicon waves. Shoji[5] has obtained almost the same results with a different antenna from that used by Boswell *et al.*[2–4] In a theoretical analysis, Chen[6,7] has suggested that the rate of energy absorption by wave damping may be due to Landau damping of the helicon wave that has an electric field component parallel to the magnetic field. This can interact directly with electrons, and hence, provides an efficient means for transferring energy to electrons that subsequently suffer inelastic collisions in the column. Landau damping has been observed and is the main subject of the present paper.

In the present paper detailed measurements are performed of the helicon wave and the efficient plasma production. Spatial variations of damping waves are measured by interferometry to obtain damping rates and wavelengths in the plasma along the magnetic field. The observed wave is consequently confirmed to obey the dispersion relation of the helicon wave, and its damping rate has the characteristics of Landau damping although the collisional damping is not negligible in our experiments. Most plasma properties observed experimentally are consistent with those predicted theoretically.

In Sec. II, we describe a theoretical background for the helicon wave. After describing in Sec. III the experimental apparatus, the observations are presented with possible interpretations in the two subsections of Sec. IV. The conclusion is given in Sec. V.

[a] Permanent address: Plasma Science Ctr., Nagoya Univ., Nagoya 464-01, Japan.

II. THEORETICAL BACKGROUND

Helicon waves are known to be right-handed circularly polarized electromagnetic waves, propagating along the magnetic field.[8–10] The frequency ω is in the range of $\omega_{ci} \ll \omega_l \ll \omega \ll \omega_{ce} \ll \omega_{pe}$, where ω_{ci} and ω_{ce} are the ion and electron cyclotron frequencies, ω_l is the lower hybrid frequency, and ω_{pe} is the electron plasma frequency. Using a cylindrical geometry (r,θ,z) and assuming the magnetic field $\mathbf{B}_0$ to be in the z direction, the helicon wave in a cylindrical plasma is described by the equations[8–10]

$$\nabla\times\mathbf{E}_1 = -\frac{\partial \mathbf{B}_1}{\partial t},\quad \nabla\times\mathbf{B}_1 = \mu_0\mathbf{j}_1,\quad \mathbf{E}_1 = \mathbf{j}_1\times\mathbf{B}_0/en_e, \tag{1}$$

where $\mathbf{E}_1$, $\mathbf{B}_1$, and $\mathbf{j}_1$ are small perturbations of the electric field, the magnetic field, and the plasma current, respectively, and n_e is the time-averaged plasma density. We assume perturbations of the form $\exp i(m\theta + kz - \omega t)$. After some algebraic manipulations, the eigenmode equation for B_{1z}, the axial component of $\mathbf{B}_1$, is obtained:[7]

$$\frac{1}{r}\frac{\partial}{\partial r}\left(\frac{r}{K^2-k^2}\frac{\partial B_{1z}}{\partial r}\right) + \left[1 - \frac{m^2}{r^2}\frac{1}{K^2-k^2} + \frac{m}{r}\frac{\partial}{\partial r}\left(\frac{1/K}{K^2-k^2}\right)\right]B_{1z} = 0, \tag{2}$$

where $K = \omega e n_e \mu_0 / k B_0$. The solution of Eq. (2) is found to be an mth order Bessel function of the first kind $J_m(\rho)$ if the uniform plasma is contained in a cylinder of radius a. We define a new variable ρ such that $\rho^2 = (K^2 - k^2)a^2$. Although the dispersion relation is determined by the boundary conditions, the same dispersion relation is obtained both in the plasma bounded by an insulator and in the plasma contained in a conducting cylinder:

$$k/K = -mJ_m(\rho)/\rho J'_m(\rho), \tag{3}$$

where $J'_m(\rho)$ is a derivative of $J_m(\rho)$. When k is smaller than A/a where A is defined as the argument which yields the first zero of $J_1(\rho)$, that is, 3.83, the dispersion relation for $m = 0$ and 1 modes is approximately given by[6,7]

$$\frac{\omega}{k} = \frac{A}{ae\mu_0}\frac{B_0}{n_e}. \tag{4}$$

 0899-8221/91/040893-06$02.00

We note that, up to here, K, k, and ρ are all real.

Since the $\mathbf{B}_1$ and $\mathbf{j}_1$ lines of the helicon wave are more or less helical, an antenna of the helical shape, that is, a helical antenna is considered to be able to excite the helicon wave by the rf at the frequency of $\omega_{ci} \ll \omega_l \ll \omega \ll \omega_{ce}$.[5] For example, an antenna consisting of two leading wires twisted helically can excite an $m = 1$ mode.

The Landau damping rate is given by[6]

$$\frac{\mathrm{Im}(k)}{\mathrm{Re}(k)} = 2\sqrt{\pi}\,\frac{c^2}{\omega_{pe}^2}\,\frac{A^2}{a^2}\,\zeta^3 \exp(-\zeta^2), \tag{5}$$

where $\zeta = \omega/kv_{\mathrm{th}}$, $v_{\mathrm{th}} = \sqrt{2k_B T_e/m_e}$, T_e is the electron temperature, and m_e is the electron mass. Equation (5) is such a steep function of ζ that a small change in T_e or k can appreciably increase the damping. Introducing the definition of ζ and inserting Eq. (4) into Eq. (5), we may write Eq. (5) as

$$\frac{\mathrm{Im}(k)}{\mathrm{Re}(k)} = 2\sqrt{\pi}\,\frac{v_{\mathrm{th}}}{\omega_{ce}}\,\frac{A}{a}\,\zeta^4 \exp(-\zeta^2). \tag{6}$$

Thus it is clear that the damping rate maximizes when $\zeta^4 \exp(-\zeta^2)$ is at its maximum value of 0.54, which occurs for $\zeta = \sqrt{2}$. Figure 1 shows the dependence of $\mathrm{Im}(k)/\mathrm{Re}(k)$ on the wavelength λ for $T_e = 3$ and 10 eV at $B_0 = 1$ kG, together with the λ dependence of n_e. The damping rates maximize surely at $\zeta (= \lambda\omega/2\pi v_{\mathrm{th}}) = \sqrt{2}$, and n_e increases monotonically with a decrease in λ. Equation (5) also says that the damping rate is inversely proportional to n_e, that is, B_0, when ζ is kept at $\sqrt{2}$. On the other hand, the damping rate due to the resistivity is given by[6]

$$\frac{\mathrm{Im}(k)}{\mathrm{Re}(k)} = \frac{\nu_{ei}}{\omega}\,\frac{c^2}{\omega_{pe}^2}\,\frac{A^2}{a^2}, \tag{7}$$

where ν_{ei} is the electron–ion collision frequency. A comparison between the damping rates represented by Eqs. (6) and (7) indicates that Landau damping is dominant in the range of $n_e \lesssim 7.2 \times 10^{12}$ cm^{-3}, while the collisional damping is larger than Landau damping in the region of $n_e \gtrsim 7.2 \times 10^{12}$ cm^{-3}; $a = 2.5$ cm, $T_e = 3$ eV, and $\omega/2\pi = 7$ MHz are used. The damping rate due to the resistivity $\mathrm{Im}(k)/\mathrm{Re}(k)$ depends little on n_e, as known from Eq. (7), and is regarded as constant within 20% in the range of 10^{12} cm$^{-3} \leqslant n_e \leqslant 10^{14}$ cm^{-3}.

III. EXPERIMENTAL ARRANGEMENT

A schematic of the experimental apparatus is shown in Fig. 2. The argon plasma produced with a helical antenna is confined in a uniform magnetic field $\mathbf{B}_0$ of up to 3 kG. The antenna is located outside the plasma, that is, on the Pyrex tube of 5 cm in diameter and 50 cm in length, which is connected to the end of the stainless-steel vacuum chamber with a length of 170 cm and an inner radius of 23 cm. The stainless-steel vacuum chamber is electrically grounded. The base pressure is kept less than 2×10^{-7} Torr, and the gas pressure p is in the range of 2×10^{-4} Torr$\leqslant p \leqslant 3 \times 10^{-3}$ Torr during the experiments. The gas inlet is located at the opposite end of the Pyrex tube to the stainless-steel vacuum chamber.

The antenna consists of two copper ribbons of 2.5 cm in width, which are wound around the Pyrex tube and have half of a winding, in order to excite an $m = 1$ mode, as shown in Fig. 2(b).[5] The length of the antenna is chosen to be 25 cm. The rf power at 7 MHz, P_{rf}, is supplied from an oscillator-amplifier system and is varied up to 2 kW. The power P_{rf} is delivered to the plasma via a coaxial cable and is matched into the antenna with two high voltage variable capacitors arranged in a π network.[3] To minimize damage to the rf circuit, the rf supply is pulsed at 83.3 Hz with a 16.7% duty

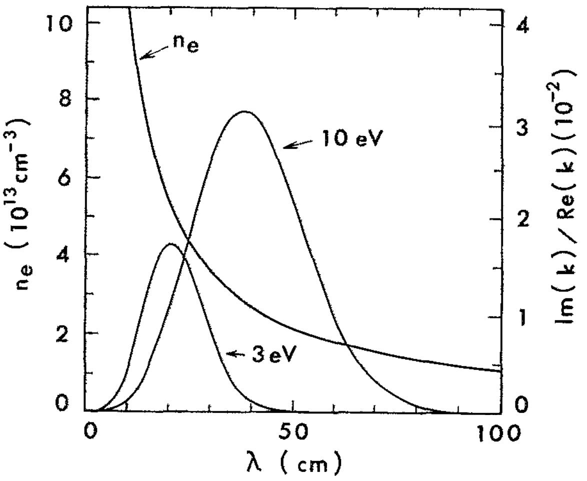

FIG. 1. Plasma density n_e and Landau damping rates $\mathrm{Im}(k)/\mathrm{Re}(k)$ for $T_e = 3$ and 10 eV, calculated using Eqs. (4) and (5) at $B_0 = 1$kG, $a = 2.5$ cm, and $\omega/2\pi = 7$ MHz.

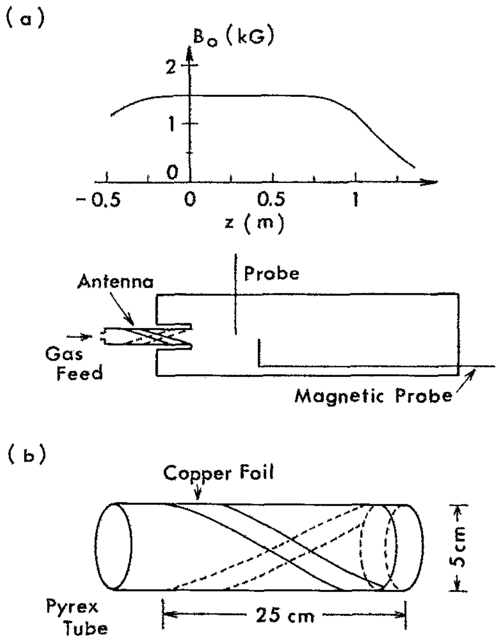

FIG. 2. Schematic of experimental apparatus. (a) Magnetic configuration $\mathbf{B}_0$ and the vacuum vessel. (b) The exciting helical antenna with half of a winding.

cycle. The plasma density n_e is measured at $t = 1.5$ msec after the oscillator is turned on at $t = 0$ msec with a boxcar integrator with a gate width of 0.1 msec, while T_e is obtained in the afterglow plasma because T_e of $4-6$ eV at $t = 1.5$ msec is considered to be affected by the rf wave.

Radial profiles of plasma parameters are measured at $z = 25$ cm, and axial profiles are obtained in the range of 25 cm$\leqslant z \leqslant$75 cm. Here, the origin of the z axis is located at the end of the Pyrex tube, which is connected to the stainless-steel vacuum chamber, as shown in Fig. 2(a). Measurements of n_e and T_e are performed with a Langmuir probe calibrated against a microwave interferometer; absolute measurements of the line-integrated electron density are made with an 8 mm microwave inteferometer. The wavelength of the helicon wave is measured by interferometry with magnetic probes, which are located inside the stainless-steel vacuum chamber, and are movable along the z axis. The magnetic probes consist of single layer solenoidal coils of 4 mm in diameter and 6 mm in length with 50 windings.

IV. EXPERIMENTAL RESULTS AND INTERPRETATION

A. Production of fully ionized plasmas

Figure 3 shows the radial profiles of n_e and T_e, measured at $p = 8\times 10^{-4}$ Torr, $P_{rf} = 0.7$ kW, and $B_0 = 0.7$ kG. It is clear that T_e is constant across the plasma, and that n_e, is almost uniform in the region inside the Pyrex tube,that is, in the region of $|r| \leqslant a = 2.5$ cm although the n_e profile depends on B_0 in practice, as will be described later. The electron temperature T_e is also found to always be 3–4 eV, and to depend little on such parameters as B_0, p, and P_{rf}.

The p dependence of n_e is shown in Fig. 4, obtained at $B_0 = 1$ kG and $P_{rf} = 1.5$ kW. The plasma density n_e is apparently proportional to p in the region of $p \lesssim 1\times 10^{-3}$ Torr, and saturates in the high-p region. Since the density n_0 of neutral argon atoms at $p = 1\times 10^{-3}$ Torr is $\sim 2.6\times 10^{13}$ cm^{-3} at the room temperature of 300 K, it is confirmed that argon atoms are completely ionized in the range of

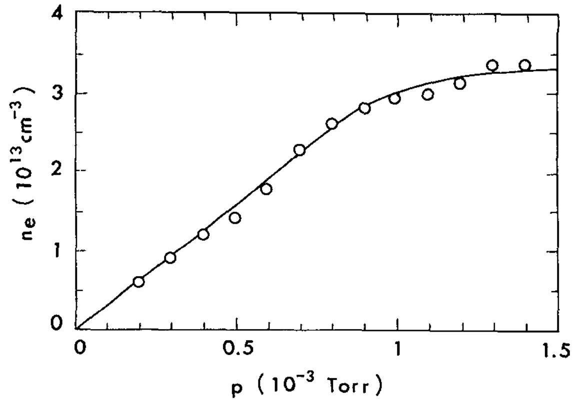

FIG. 4. Dependence of n_e on p at $B_0 = 1$kG and $P_{rf} = 1.5$ kW.

$p \lesssim 1\times 10^{-3}$ Torr. The reason why n_e is a little larger than n_0 in the range of $p \lesssim 1\times 10^{-3}$ Torr, is attributed to the fact that p is measured at the position close to the vacuum pump rather than the gas inlet. In the high-p region, it is considered that there is not enough rf power for all neutral atoms to be ionized. In this case, the discharge color is found to be light pink arising from the many lines of neutral argon in the red part of the spectrum. On the other hand, the color of the central volume is dark blue due to emission of Ar II lines when the fully ionized plasma is achieved.

Figure 5 shows the dependence of n_e on P_{rf} for various B_0's. The gas pressure p is kept at 8×10^{-4} Torr in the rest of this paper except for the experiments to obtain Fig. 9. It is found that the large rf power is required to some extent in order to realize the fully ionized plasma, and B_0 affects the plasma production seriously in the manner that the larger B_0 makes it easier to achieve 100% ionization. In our system, it is difficult for the matching between the plasma and rf circuit

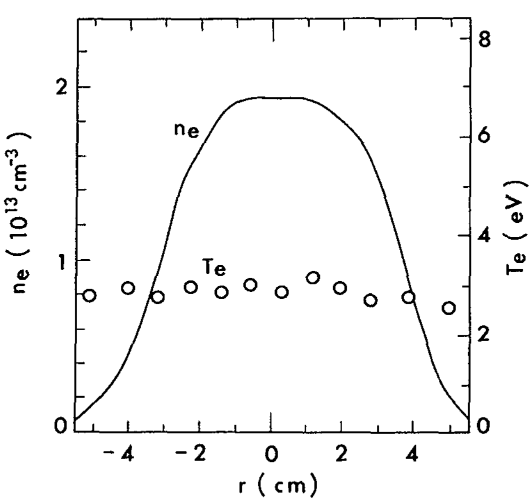

FIG. 3. Radial profiles of n_e and T_e, measured at $p = 8\times 10^{-4}$ Torr, $P_{rf} = 0.7$ kW, and $B_0 = 0.7$ kG.

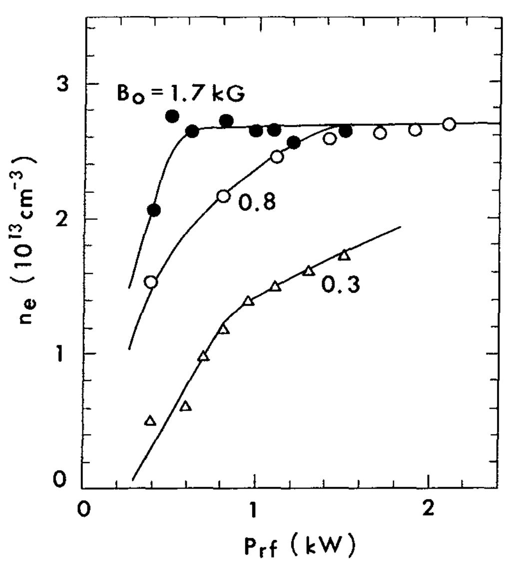

FIG. 5. Dependence of n_e on P_{rf} for various B_0's.

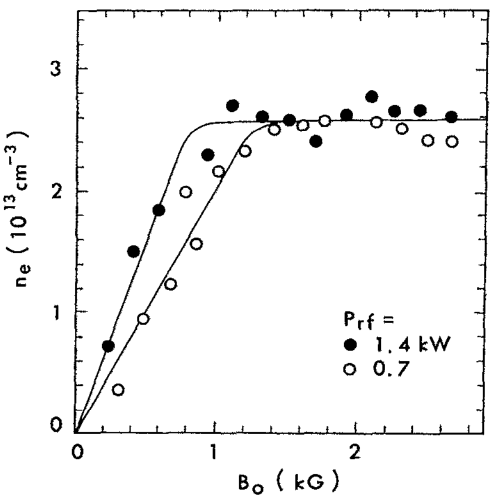

FIG. 6. Density n_e as a function of B_0 for $P_{rf} = 0.7$ and 1.4 kW.

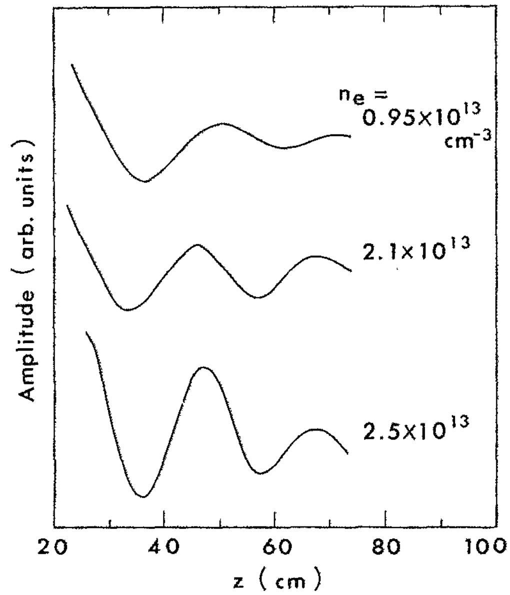

FIG. 8. Tracings of spatial variations of damped waves; B_0/n_e's are 4.2×10^{-14} kG cm^3, 3.5×10^{-14} kG cm^3, and 3.2×10^{-14} kG cm^3 from the top.

to be adjusted at P_{rf}'s below $\sim$0.4 kW, so that we cannot produce the plasma in this P_{rf} range.

The B_0 dependence of n_e is shown in Fig. 6 for $P_{rf} = 0.7$ and 1.4 kW. The electron density n_e is roughly proportional to B_0 in the region of $B_0 \lesssim 1$ kG, although the slope of the curve depends a little on P_{rf}. This agrees qualitatively with the relation between n_e and B_0, predicted in the dispersion relation of the helicon wave. For quantitative agreement, the measurement of the wavelength is, of course, required, as known from Eq. (4). In the range of $B_0 \gtrsim 1$ kG, n_e is constant independently of B_0 since the fully ionized plasma is accomplished. The radial n_e profile is studied by changing B_0 at $P_{rf} = 1.4$ kW, and the result is shown in Fig. 7. When B_0 is smaller than $\sim$0.45 kG, the n_e profile around $r = 0$ cm has a concave shape and the distance betwen two ridges is almost equal to the inner diameter of the Pyrex tube. By increasing B_0, the n_e profile is varied drastically and becomes peaked at $r = 0$ cm, as shown in Fig. 7. This dependence of the radial n_e profile on B_0 may be explained by

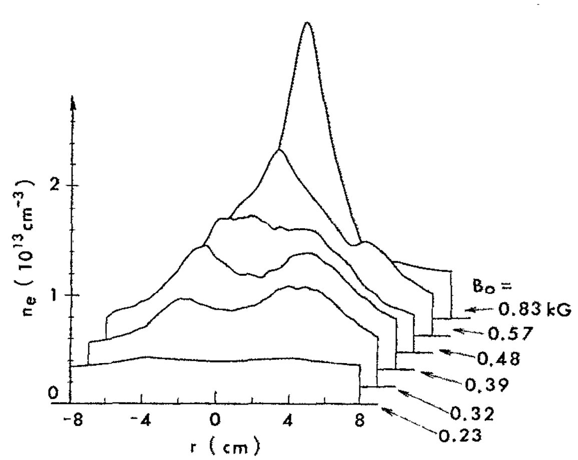

FIG. 7. Dependence of radial n_e profile on B_0 at $P_{rf} = 1.4$ kW.

taking account of the confinement of the plasma.[6] Basically, the heating and ionization will be localized near the walls, and so is the energy deposition. This causes the concave n_e profile with the ridges at the inner-wall position of the Pyrex tube. By increasing B_0, the energy confinement, which is determined by the end plate sheaths and the intensity of $\mathbf{B}_0$, may be better on the axis, leading to the appearance of a dense core.

B. Dispersion relation and damping of the helicon wave

The phase and amplitude of the helicon wave as a function of axial position z are obtained by interferometry with the magnetic probe. Tracings of the spatial variations of the damped waves are shown in Fig. 8 at $B_0 = 0.4 - 0.8$ kG and $P_{rf} = 1.3 - 1.6$ kW. An important point in the figure is that the wavelength is about half of the antenna length, and is varied depending on n_e, strictly speaking, on B_0/n_e as expected from Eq. (4). This suggests that the wavelength is not determined by the antenna length, and is varied automatically to provide the best coupling or to satisfy the dispersion relation. We cannot obtain the dispersion relation directly since the frequency of the oscillator is fixed, but the relation between n_e and kB_0 can be obtained, and compared with the theoretical prediction. Figure 9 shows the dependence of n_e on kB_0 under various conditions of B_0, P_{rf}, and p. The experimental results represented by open circles are obtained in the low-B_0 region, where n_e does not saturate with the variation of B_0 and the relatively flat n_e profile is observed inside the Pyrex tube. The solid line represents n_e given by Eq. (3); $a = 2.5$ cm and $\omega/2\pi = 7$ MHz are used. It is evident that n_e is proportional to kB_0, and there is relatively good agreement between the experimental and theoretical results, indicating that the observed wave obeys the dispersion relation of the helicon wave.

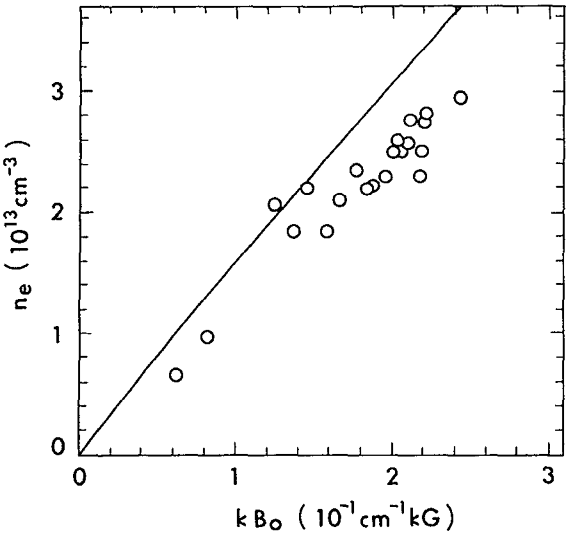

FIG. 9. Dependence of n_e on kB_0 under various conditions of B_0, P_{rf}, and p.

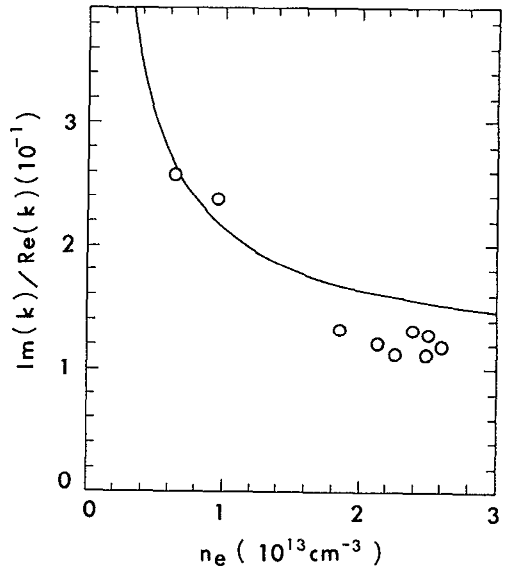

FIG. 10. Dependence of Im(k)/Re(k) on n_e, obtained by changing B_0 at $P_{rf} = 1.5$ kW.

The most important point which is noticed in studying the relation between n_e and k, is that ζ approaches $\sqrt{2}$ by increasing n_e and keeping B_0 constant, and that n_e has a maximum at $\zeta \sim \sqrt{2}$ where the Landau damping rate maximizes. In fact, the lowest tracing in Fig. 8 yields $\zeta = 1.49 \sim \sqrt{2}$ at $T_e = 3$ eV and $\omega/2\pi = 7$ MHz. This suggests that the damping of the helicon wave can be explained by Landau damping in our experiments. The variation of B_0 makes it possible to change n_e with keeping ζ at $\sim \sqrt{2}$.

The value of Im(k)/Re(k) can be also obtained from the tracing of the spatial variation of the damped wave. Figure 10 shows the dependence of Im(k)/Re(k) on n_e, obtained by changing B_0. The wave number k is kept constant to satisfy $\zeta = \sqrt{2}$, as mentioned above. The experimental results are plotted by open circles. There is a tendency for Im(k)/Re(k) to decrease with an increase in n_e. This is characteristic of Landau damping, and cannot be explained by the collisional damping since Im(k)/Re(k) due to the resistivity depends little on n_e, as known from Eq. (7). However, for example, at $n_e = 2.5 \times 10^{13}$ cm^{-3}, the Landau damping rate is about one third of the collisional damping rate, and is about one-fourth of the measured damping rate. Landau damping is larger than the collisional damping in the range of $n_e \lesssim 7.2 \times 10^{12}$ cm^{-3}. Taking account of these results, both Landau damping and collisional damping are considered to occur at the same time in our n_e range. The solid line shown in Fig. 10 represents the damping rate predicted theoretically, which consists of the Landau damping rate plus the collisional damping rate. Good agreement is found between the experimental and theoretical results.

V. CONCLUSIONS

Experiments reported here demonstrate the excitation of a helicon wave in a cylindrical magnetoplasma and the production of a fully ionized plasma. An axial wavelength measured in the vacuum chamber indicates that the axial wavelength is not determined by the antenna length, but is automatically varied depending on the density and the magnetic field to satisfy the dispersion relation of the helicon wave. As the magnetic field is increased, the density increases according to the dispersion relation of the helicon wave, and the central core of the plasma becomes fully ionized at an appreciable rf power with the optical emissions being typical of Ar II. It is also shown that the density has a maximum at $\zeta(= \omega/kv_{th}) \sim \sqrt{2}$ where the Landau damping rate maximizes, and that there is a tendency for Im(k)/Re(k) to decrease with an increase in the density. These are characteristic of Landau damping. However, both Landau damping and collisional damping are considered to occur at the same time in our density range, since the collisional damping rate is larger than the Landau damping rate at densities above 7.2×10^{12} cm^{-3}. There is good agreement between the experimental and theoretical damping rates when the theoretical damping rate consists of both the Landau damping rate and the collisional damping rate. Landau damping rather than the collisional damping is considered to play an important role on the plasma production, because the resonant mechanism can accelerate electrons to ionizing energies more efficiently.

ACKNOWLEDGMENTS

The authors wish to thank M. Tanaka for many illuminating discussions, and M. Fujiwara, N. Sato, and H. Ikegami for their continuing encouragement.

This work was supported by a Grant-in-Aid for Scientific Research from the Ministry of Education, Science and Culture of Japan.

[1]G. Lisitano, R. A. Ellis, Jr., W. M. Hooke, and T. H. Stix, Rev. Sci. Instrum. **39**, 295 (1968).
[2]R. W. Boswell, R. K. Porteous, A. Prytz, A. Bouchoule, and P. Ranson, Phys. Lett. A **91**, 163 (1982).
[3]R. W. Boswell, Plasma Phys. Controlled Fusion **26**, 1147 (1984).
[4]Z. Peiyuan and R. W. Boswell, Phys. Rev. Lett. **63**, 2805 (1989).
[5]See AIP document No. PAPS-PFBPE-03-893-7 for 7 pages of "Whistler Wave Plasma Production," by Tatsuo Shoji, Annual Review, Institute of Plasma Physics, Nagoya University, Japan (1986), p. 67. Order by PAPS number and journal reference from American Institute of Physics, Physics Auxiliary Publication Service, 335 East 45th Street, New York, NY 10017. The price is $1.50 for each microfiche (98 pages) or $5.00 for photocopies of up to 30 pages, and $0.15 for each additional page over 30 pages. Airmail additional. Make checks payable to the American Institute of Physics.
[6]F. F. Chen, in *Proceedings of the Second International Conference on Plasma Physics*, Kiev 1987, edited by A. G. Sitenko (Naukova Dumka, Kiev, 1987), Vol. 4, p. 321.
[7]F. F. Chen and C. D. Decker, Bull. Am. Phys. Soc. **34**, 2128 (1989); F. F. Chen, Laser Part. Beams **7**, 551 (1989).
[8]J. A. Lehane and P. C. Thonemann, Proc. Phys. Soc. London **85**, 301 (1965).
[9]G. N. Harding and P. C. Thonemann, Proc. Phys. Soc. London **85**, 319 (1965).
[10]J. P. Klozenberg, B. McNamara, and P. C. Thonemann, J. Fluid Mech. **21**, 545 (1965).